Efficient Integral Equation Analysis of 3-D Rectangular Waveguide Microwave Circuits by Using Green's Functions Accelerated With the Ewald Method

Antonio Manuel Huéscar de la Cruz, *Student Member, IEEE*, Celia Gómez Molina, Fernando Daniel Quesada Pereira, *Member, IEEE*, Alejandro Álvarez Melcón, *Senior Member, IEEE*, and Vicente E. Boria Esbert, *Fellow, IEEE*

***Abstract*— In this contribution, an electric field integral equation (EFIE) formulation is proposed, for the analysis of microwave circuits based on rectangular waveguides with an unlimited number of arbitrarily 3-D-shaped conducting elements. For this purpose, the Lorenz gauge rectangular waveguide Green's functions are used. Moreover, the Ewald method has been employed to significantly speed up the evaluation of these rectangular waveguide Green's functions. Strategies are also proposed to switch between different ways of calculating the Green's functions depending on the source-observation distance along the propagation direction. In addition, the method of moments (MoM) has been applied to solve the EFIE. Following the application of this technique, the impedance matrix resulting from the MoM has been divided into dynamic and static parts, thus reducing the computational time required to obtain the frequency response of practical 3-D microwave circuits by up to a factor of 3 compared with the traditional formulation. On the other hand, a generic expression is derived to evaluate the multimode scattering parameters of rectangular waveguide circuits, independently on the mode used to excite the structure. The evaluation of the electromagnetic fields inside the rectangular waveguides has also been carried out. The proposed technique has been validated by comparison with results provided by commercial full-wave software, such as ANSYS HFSS and CST Studio Suite, showing good agreement and good numerical efficiency.**

***Index Terms*— Electric field integral equation (EFIE), electromagnetic field evaluation, Ewald method, Green's function, method of moments (MoM), rectangular waveguide circuits, scattering parameters.**

Manuscript received 9 March 2024; accepted 9 April 2024. Date of publication 25 April 2024; date of current version 7 October 2024. This work was supported in part by the Spanish Ministerio de Ciencia e Innovación in the framework of the research projects: "Design and Development of New High-Performance Components for High-Frequency Communication Systems (NEWCOSYS)" under Grant PID2022-136590OB-C42 and "Advancing on Waveguide Technologies for Near-Future Satellite Communication Equipment (ADWASAT)" under Grant PID2022-136590OB-C41; in part by the Agencia Estatal de Investigación, European Union Next Generation Funds in the projects "Antennas and Circuits for Efficient Wireless Sensor Networks Using Low-Orbit Satellites (ARIELS)" under Grant TED2021-129196B-C42 and "Technological Demonstrator of New Radio Links Between Small Satellites and Earth Stations for Advanced Digital Applications (CHILD-SAT)" under Grant TED2021-129196B-C41; and in part by the Fundación Séneca, Agencia de Ciencia y Tecnología de la Región de Murcia, Spain, through "Componentes radiantes y de filtrado de microondas para satélites emergentes" under Project 22076/PI/22. *(Corresponding author: Fernando Daniel Quesada Pereira.)*

Antonio Manuel Huéscar de la Cruz, Fernando Daniel Quesada Pereira, and Alejandro Álvarez Melcón are with the Department of Communications and Information Technologies, Universidad Politécnica de Cartagena, 30202 Cartagena, Spain (e-mail: antoniomanuel.huescar@edu.upct.es; fernando.quesada@upct.es; alejandro.alvarez@upct.es).

Celia Gómez Molina is with Ansys Iberia, 28046 Madrid, Spain (e-mail: celia.gomezmolina@ansys.com).

Vicente E. Boria Esbert is with the Research Development Institute on Telecommunication and Multimedia Applications, Universitat Politècnica de València, 46022 Valencia, Spain (e-mail: vboria@dcom.upv.es).

Color versions of one or more figures in this article are available at https://doi.org/10.1109/TMTT.2024.3388193.

Digital Object Identifier 10.1109/TMTT.2024.3388193

I. Introduction

In RECENT decades, microwave devices in waveguide technology [1] have increasingly been used as an alternative to microwave circuits in planar technologies, as they have considerably low losses and are capable of handling high-power levels in applications, such as space communications systems [2], [3]. In addition, these circuits can be composed of a high number of arbitrarily shaped metallic and/or dielectric elements within them [4], [5], [6] in order to achieve the desired performance. The popularization of this type of devices has favored the research of different numerical techniques, such as those based on finite difference in time domain (FDTD), finite elements, or integral equations (IEs) solved by the method of moments (MoM) [7], [8], [9], [10]. These techniques allow the evaluation of the electromagnetic fields inside the structures and also the calculation of their circuit responses, i.e., their scattering parameters. The FDTD and finite element method (FEM) [7], [8] are suitable for the analysis of very complex geometries, since they apply a full discretization of arbitrarily shaped structures by means of adaptive meshes. The main problem with such numerical methods is the need of a large memory storage and their associated computational cost. On the other hand, the use of modal techniques should also be highlighted. These techniques are very fast, but have the disadvantage that they are limited to the analysis of a certain type of canonical geometries [11],

© 2024 The Authors. This work is licensed under a Creative Commons Attribution 4.0 License.
For more information, see https://creativecommons.org/licenses/by/4.0/

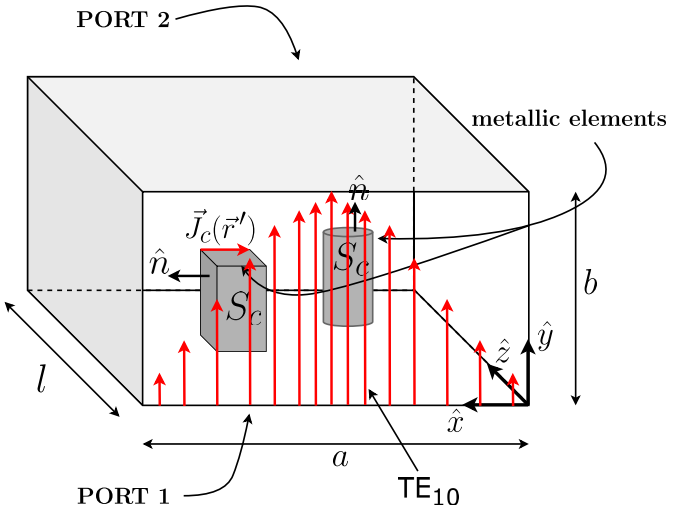

Fig. 1. Sketch of a generic rectangular waveguide, with dimensions $a \times b$ in the XY plane and with a length l along the z-axis, including two arbitrarily shaped conducting elements inside it.

[12], [13]. In addition, there exist other strategies, such as those shown in [14] and [15], where numerical techniques based on mode matching (MM) are proposed. In [14], a hybrid strategy between the FEM and MM together with the use of a modified transverse resonance (MTR) technique is shown, which provides accurate results but requires dense meshing.

On the other hand, IE [9] methods can also analyze complex structures, with the advantage that they can be formulated to require only the mesh of discrete objects acting as discontinuities in a given reference geometry. In fact, the boundary conditions of the reference structure containing these objects are included in especially tailored Green's functions. Other IE techniques, such as those shown in [16], [17], and [18], are based on the boundary integral-resonant mode expansion (BI-RME) method. This numerical technique, after solving an eigenvalue problem, provides an efficient procedure to obtain the wideband response of guided circuits under analysis. As disadvantages, the analysis of structures in the presence of dielectric objects, electrically large structures with step discontinuities between different rectangular waveguides, becomes complex as well as computationally expensive. At this point, where there exist electrically large structures, segmentation techniques could be applied to split the main problem into smaller, more manageable problems, but this increases complexity. Another complex task for this type of formulation is the evaluation of the electromagnetic field inside these structures for a specific frequency. Therefore, it may not be an optimal technique to study phenomena, such as corona or multipactor [2], [3].

In this contribution, we propose an efficient electric field IE (EFIE) [9] formulation for the analysis of 3-D rectangular waveguide circuits with arbitrarily shaped perfect electric conducting (PEC) objects, as shown in Fig. 1. In this formulation, the boundary conditions on the walls of the rectangular waveguide are modeled by the corresponding Green's functions introduced in the IE kernel. Subsequently, the EFIE is solved only on the arbitrarily shaped metallic objects by the MoM [10], using a given combination of rooftop and/or Rao–Wilton–Glisson (RWG) basis and test functions (Galerkin approach), defined, respectively, on rectangular and triangular mesh elements [19], [20], [21]. Moreover, as previously mentioned for IE techniques, an important advantage of this type of formulation is that it does not require a complete mesh of the whole volume to be analyzed, as it is the case for FEM or FDTD techniques, which greatly reduces the number of unknowns to be solved. Although the focus in this article will be on EFIE, this IE formulation could also be extended to a magnetic field IE (MFIE) or a combined field IE (CFIE).

A difficulty of the proposed IE technique is that its efficiency is limited by the slow convergence of spectral or spatial images series, associated with the evaluation of the rectangular waveguide Green's functions [22]. To reduce as much as possible this computational cost, the Ewald method will be used, which properly combines both spectral and spatial images series in a convenient formulation [23]. In [24], this method is extended to the efficient computation of rectangular waveguide Green's functions derivatives, which will be used in this article for the evaluation of electromagnetic fields inside the structures.

Even though the computational cost in the evaluation of the Green's functions of the rectangular waveguide is reduced, the *bottleneck* of this EFIE technique is still in the calculation of the moment matrix elements. Therefore, to further improve the efficiency, we propose, in this article, to split the original moment matrix into two parts, one dynamic and one static. This technique is focused on evaluating the dynamic part of the moment matrix, which is nonsingular and frequency-dependent, as fast as possible. On the other hand, the static part, which has singular elements, is slower, but since it is frequency-independent, it is computed only once during the frequency analysis of a given device. In this article, we introduce, as a novelty different options to compute the dynamic part of the matrix, by substracting different image distributions to the total Green's functions evaluated with the improved technique based on the Ewald method reported in [24].

The first challenge to apply this method is the calculation of the singular elements of the static moment matrix, resulting from the self-interaction between basis and test functions defined on the same mesh cell. To increase the efficiency for these interactions, the contribution of the singular $(1/R)$ term of the potential Green's functions is separated, and the corresponding integral with the basis and test functions is analytically evaluated [25], [26].

The second challenge is how to compute efficiently the dynamic part of the moment method. Even though this part has no singularities, the self-interactions between basis and test functions are still nondifferentiable, and a direct numerical integration only converges with a large number of points. To reduce the numerical effort needed to compute these nondifferentiable elements, in this article, we propose a division of the self-interaction cells into subtriangles, taking each observation point as the subdivision vertex.

The rest of the MoM elements, both static and dynamic, are evaluated numerically using cubature rules defined in canonical integration domains, as explained in [27]. For these

interactions, we also introduce a new strategy to increase the efficiency. The strategy is based on switching between different techniques to evaluate the Green's functions of the base rectangular waveguide, depending on the electrical source-observation distance.

This article is organized as follows. First, Section II has been divided into four different sections. Section II-A will give a brief overview of the EFIE to facilitate the understanding of the aspects to be improved in this formulation. After that, Section II-B will show how to carry out the procedure of separating the EFIE moment matrix into static and dynamic parts. Furthermore, this section will discuss the different ways to evaluate the dynamic part by substracting different arrangements of spatial images. This section also covers the strategy used to calculate the nondifferentiable elements of the resulting dynamic moment matrix corresponding to the self-interactions of the dynamic part. The strategy proposed to increase efficiency in the calculation of the rest of the elements (both static and dynamic) is covered in Section II-C. The technique is based on switching between several different ways to evaluate the Green's functions of the rectangular waveguide, depending on the electrical source-observation distance. To conclude the theoretical part of this work, it will be shown how to evaluate the multimode scattering parameters of a given microwave component, once the IE is solved.

Next, in Section III, some results obtained with the theory developed throughout Section II will be shown. In Section III-A, the effects of using the different options discussed in Section II-B to extract the singularity from the dynamic MoM matrix are discussed in terms of computational cost and accuracy. This study will be very important to improve the efficiency of the numerical implementation without compromising the accuracy. Then, in Section III-B, the proposed technique will be applied to the computation of the scattering parameters of different practical devices in rectangular waveguides. These results will be compared with those provided by commercial full-wave software packages, such as ANSYS HFSS [28] and CST Studio Suite [29]. To conclude this section, in Section III-C, a comparison of the electromagnetic fields inside a filter in rectangular waveguide technology between the IE method employed in this work and ANSYS HFSS will be shown. Finally, in Section IV, the conclusions of this work and some future research lines will be discussed.

II. Theory

A. Electric Field Integral Equation in Rectangular Waveguides

In this section, we begin by briefly outlining the EFIE formulation used in this work, whose implementation is well known for studying radiation from both open and closed conducting structures. This formulation is based on the solution of an IE where the unknown is the surface electric current density induced on the perfect conducting structure, whereas the enforced boundary condition is the nullity of the total electric field tangent to its external surface (S_c), as shown in Fig. 1.

In this IE formulation, in order to alleviate the mathematical singularities resulting from working directly with Maxwell's electromagnetic field expressions [30], we resort to make use of auxiliary potential functions, such as those used in [31]. Thus, the electric field scattered by a perfect conductor can be written as follows:

$$\vec{E}^s(\vec{r}) = -j\omega\vec{A}(\vec{r}) - \nabla\phi_e(\vec{r}) \tag{1}$$

where $\vec{A}(\vec{r})$ is the magnetic vector potential, $\phi_e(\vec{r})$ is the electric scalar potential, and $\vec{r}$ is the observation point where the electromagnetic field is evaluated.

It should be noted that the potential functions, in addition to being dependent on the position of the source ($\vec{r}\,'$) and of the observer ($\vec{r}$), are also dependent on the frequency.

The electric field of the structure will be the sum of the electric field scattered by the structure $\vec{E}^s(\vec{r})$, as shown in (1), and the electric field produced by the excitation sources $\vec{E}^i(\vec{r})$. Thus, the EFIE can be written as follows:

$$\hat{n} \times (\vec{E}^i + \vec{E}^s)\big|_{S_c} = 0 \tag{2}$$

where S_c is the conductor surface, where the boundary condition is imposed, and $\hat{n}$ is the unit vector normal to the conducting surface (see Fig. 1).

Next, to solve the EFIE, the MoM [10] is applied, in which the unknown electric current surface density $[\vec{J}_c(\vec{r})]$ is expanded as the sum of weights (a_n), whose values have to be determined, multiplied by a finite set of basis functions, which, in our case, will be rooftop for rectangular mesh cells [20] or RWG for triangular mesh cells [19], [21].

The next step is to transform the EFIE into a system of linear equations. First, the generalized impedance moment matrix is obtained, which relates the voltage and current induced in every element used in the discretization of the structure under study. To obtain this impedance matrix (Z_{mn}), a test procedure must be applied, obtaining

$$\begin{aligned} Z_{mn} = {} & j\omega \int_{S_m} \vec{f}_m(\vec{r}) \cdot \left(\int_{S_n} \overline{\overline{G}}_A(\vec{r}, \vec{r}\,')\vec{f}_n(\vec{r}\,')\, dS' \right) dS \\ & - \tfrac{j}{\omega} \int_{S_m} \nabla \cdot \vec{f}_m(\vec{r}) \left(\int_{S_n} G_V(\vec{r}, \vec{r}\,') \nabla' \cdot \vec{f}_n(\vec{r}\,')\, dS' \right) dS \end{aligned} \tag{3}$$

where S_n and S_m are the mesh cells where the basis $\vec{f}_n(\vec{r}\,')$ and test functions $\vec{f}_m(\vec{r})$ are defined. In the case of this article, the set of test and basis functions will be the same (Galerkin approach). It should be noted that in (3), it has been possible to apply the divergence operator to the test function, because the selected test functions are "divergence conforming" with continuity on the common edge. As shown, the divergence finally affects to the test functions, instead of affecting to the electric scalar potential $G_V(\vec{r}, \vec{r}\,')$, thus avoiding higher order singularities in the Green's functions.

Next, the vector of independent terms of the problem that is related to the excitation of the structure is constructed. Its elements are calculated by solving the following test integral:

$$e_m = \int_{S_m} \vec{f}_m(\vec{r}) \cdot \vec{E}^i(\vec{r})\, dS \tag{4}$$

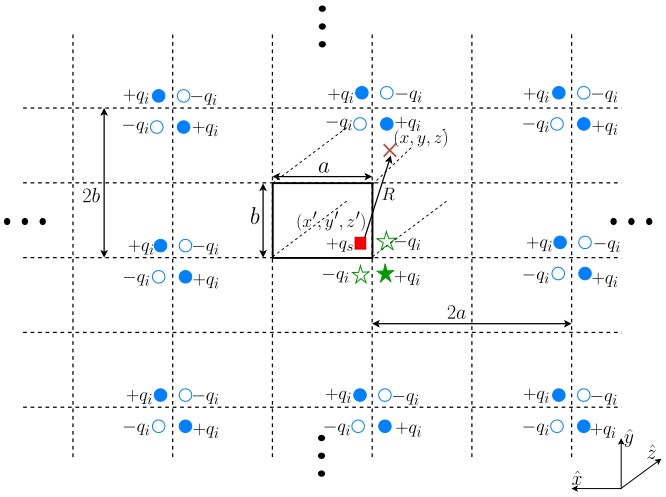

Fig. 2. Static discrete image distribution for the evaluation of the auxiliary function G_{stat}. The different configurations to be considered in this work are as follows: considering only the source term (red square), the first quartet of images corresponding to the source (red square plus green stars), and up to the first layer of images (red square, green stars, and blue circles).

where $\vec{E}^i$ is the excitation field (usually the TE_{10} fundamental mode of the rectangular waveguide).

B. Efficient Filling of the Generalized Impedance Moment Matrix

In this section, it will be shown how to reduce the computational time required for the calculation of the impedance MoM matrix presented in Section II-A. To do so, we remark that the bottleneck of this formulation is located in the evaluation of the Green's functions present in the calculation of this matrix.

To overcome this problem, on the one hand, an efficient evaluation of the Green's functions will be carried out by using the Ewald method acceleration technique. The strategies shown in [23] and [24] have been employed to make a more efficient use of the Ewald method. On the second hand, the Green's functions of the rectangular waveguide will be divided into static and dynamic parts, giving rise in the IE algorithm to the static and dynamic moment matrices ($[Z_{mn}^{\text{stat}}]$, $[Z_{mn}^{\text{dyn}}]$), as follows:

$$Z_{mn}^{\text{stat}} = j\omega \int_{S_m} \vec{f}_m(\vec{r}) \cdot \left(\int_{S_n} \overline{\overline{P}}_{\text{stat}}(\vec{r}, \vec{r}') \vec{f}_n(\vec{r}')\, dS' \right) dS - \frac{j}{\omega} \int_{S_m} \nabla \cdot \vec{f}_m(\vec{r}) \left(\int_{S_n} G_{\text{stat}}(\vec{r}, \vec{r}') \nabla' \cdot \vec{f}_n(\vec{r}')\, dS' \right) dS \tag{5}$$

$$Z_{mn}^{\text{dyn}} = j\omega \int_{S_m} \vec{f}_m(\vec{r}) \cdot \left(\int_{S_n} \left(\overline{\overline{G}}_A(\vec{r}, \vec{r}') - \overline{\overline{P}}_{\text{stat}}(\vec{r}, \vec{r}') \right) \cdot \vec{f}_n(\vec{r}')\, dS' \right) dS - \frac{j}{\omega} \int_{S_m} \nabla \cdot \vec{f}_m(\vec{r}) \cdot \left(\int_{S_n} \left(G_V(\vec{r}, \vec{r}') - G_{\text{stat}}(\vec{r}, \vec{r}') \right) \nabla' \cdot \vec{f}_n(\vec{r}')\, dS' \right) dS. \tag{6}$$

As shown, the dynamic moment matrix is obtained by substracting a singularity term also called static part ($\overline{\overline{P}}_{\text{stat}}$ or G_{stat}) to the total Green's functions ($\overline{\overline{G}}_A$ and G_V) evaluated with the Ewald technique. Since the dynamic moment matrix has no singularities, the integration of these elements can be evaluated by means of optimal numerical cubature rules defined in triangles or rectangles [27], with a reduced number of integration points.

In this work, we have assessed the efficiency of defining the singularity term (static part) using different options, as follows.

1) Define the static part ($\overline{\overline{P}}_{\text{stat}}$ or G_{stat}) with the whole static Green's functions of the rectangular waveguide accelerated with the Ewald method.
2) Define the static part, using the spatial images representation, only as the source term (see the red square in Fig. 2), which can then be integrated analytically as in [25] and [26].
3) Define the static part using the spatial images representation. However, in this case, we include, in the static part, the source term and the first quartet of spatial images (red square and green stars in Fig. 2).
4) Define the static part again using the spatial images representation. In this case, we include, in the static term, the source term and up to the first layer of images (red square, green stars, and blue circles in Fig. 2).

A study of the different options for defining the static part of the Green's functions is necessary, in order to know which one leads to more accurate results and to a more efficient evaluation. For this analysis, a standard WR-90 rectangular waveguide of dimensions ($a = 22.86$ mm $\times$ $b = 10.16$ mm), as shown in Fig. 3(a), has been taken as an example. A source point has been placed at $(x', y') = (2 \text{ mm}, 2 \text{ mm})$, and 500 observation points along the x-axis, at a height $y = 2.64$ mm and at a distance along the propagation axis of $|z - z'| = 1$ mm, were taken. For the first option, based on the application of the Ewald method to the total static summation, the number of modes used in the summation of the spectral part was 12, while for the spatial part series, a single layer of images (the red square, the green stars, and the blue circles in Fig. 2) was taken. With these parameters, the result converges rapidly. On the other hand, the working frequency is $f = 10$ GHz.

As can be seen in Fig. 3(b), when subtracting the static part from the total Green's functions, the dynamic part is smooth with practically all the proposed methods (except when extracting only the source). However, in another study performed with the source coordinates centered with respect to the walls of the rectangular waveguide (source coordinates $(x', y') = (11.43 \text{ mm}, 5.08 \text{ mm})$ and the 500 observation points distributed along the x-axis located at a height $y = 9.14$ mm and a distance along the propagation axis of $|z - z'| = 1$ mm), it can be seen that taking only the first quartet of images leads to nonoptimal results, as shown in Fig. 4. Following these results, it is concluded that only the static Ewald method and the static discrete image distribution up to the first layer will be valid options for evaluating $\overline{\overline{P}}_{\text{stat}}$ and G_{stat}.

Following this strategy, an efficient evaluation of the dynamic moment matrix is possible. This is due to the fact that by extracting the static part of the Green's functions, a very smooth behavior remains for the dynamic term,

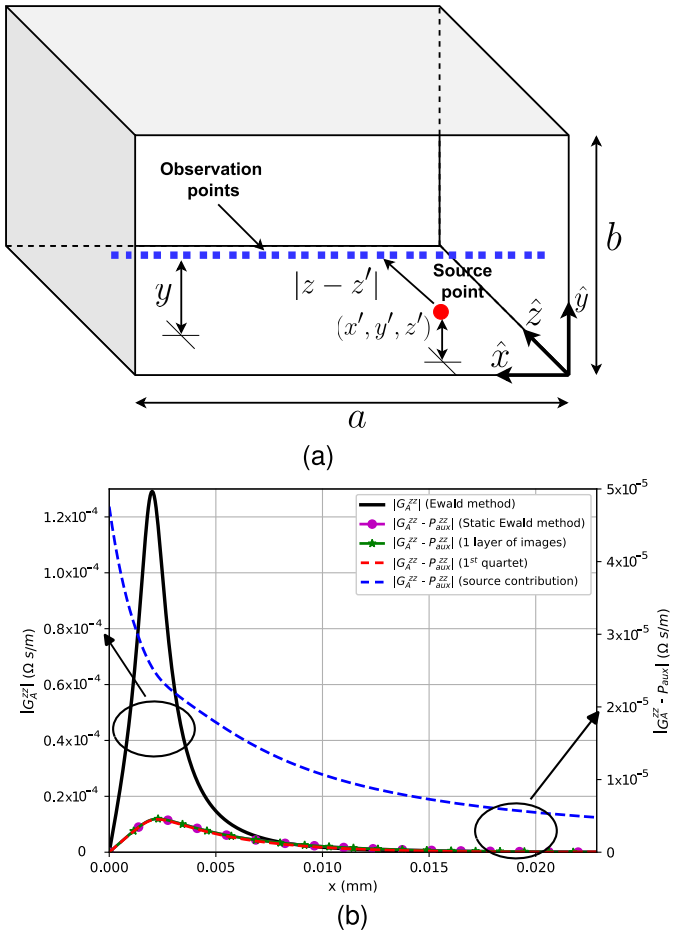

Fig. 3. (a) Sketch of a standard WR-90 rectangular waveguide, with dimensions $a = 22.86$ mm $\times$ $b = 10.16$ mm in the XY plane. This includes the location of a source point at coordinates $(x',\ y') = (2$ mm, 2 mm) and a distribution of observation points along the x-axis, at a height $y = 2.64$ mm from the bottom wall of the rectangular waveguide and at a distance from the source point in the propagation direction of $|z - z'| = 1$ mm. (b) Representation of a x-axis cut of the magnitude of the magnetic vector potential Green's function dyadic component G_A^{zz} using the Ewald method, as shown in Fig. 3(a). The rest of the curves shows at the same cut, the difference between the G_A^{zz} component and the different choices used to evaluate the P_{aux}^{zz}. G_V has a very similar behavior to G_A^{zz}.

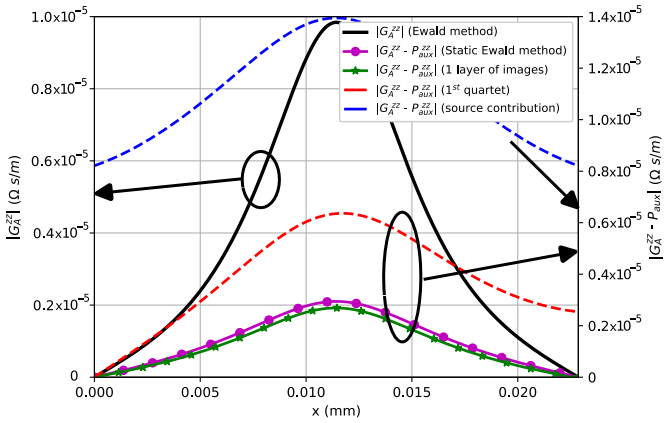

Fig. 4. Representation of a x-axis cut of the magnitude of the magnetic vector potential Green's function dyadic component G_A^{zz} using the Ewald method, as shown in Fig. 3(a). The rest of the curves shows at the same cut, the difference between the G_A^{zz} component and the different choices used to evaluate the P_{aux}^{zz}. The source coordinates are $(x',\ y') = (11.43$ mm, 5.08 mm), and the 500 observation points distributed along the x-axis are located at a height $y = 9.14$ mm and a distance along the propagation axis of $|z - z'| = 1$ mm.

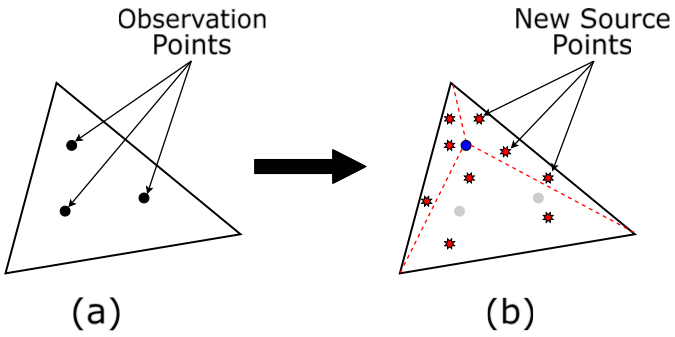

Fig. 5. Process of subdividing mesh cells into subtriangles, when self-interaction of test and basis functions occurs in the same mesh cell. (a) Observation points in the original mesh cell can be seen (black circles). (b) Subtriangles with the new source points (red stars), for an original observation point (blue circle). In (b), it should be noted that the new source points appearing in each subtriangle are only for one original observation point. In this example, the process of division into subtriangles would have to be repeated for the other original observation points (gray circles).

as demonstrated in Fig. 3(b). Therefore, the elements of the dynamic moment matrix (6) can accurately be evaluated with low-order quadrature rules.

Still, the evaluation of the dynamic moment matrix involves nondifferentiable elements for the interaction between basis and test functions defined on the same mesh cells. We have verified that a direct integration of these elements needs a large number of integration points. Therefore, to evaluate these nondifferentiable elements of the dynamic matrix efficiently, a technique based on dividing the cells into subtriangles for each observation point is employed, as illustrated in Fig. 5. In this technique, for each of the original observation points [see Fig. 5(a)], it is divided into subtriangles, and at each of these subtriangles, the new source integration points are calculated, as can be seen in Fig. 5(b). Therefore, for the specific example in Fig. 5, three source integrals (one for each subtriangle) would be performed for each original observation point. Subsequently, the integral for each observation point would be the sum of the three subtriangles.

On the other hand, the efficiency of the evaluation of the static moment matrix (5) will be closely related to the way in which the auxiliary functions $\overline{\overline{P}}_{\text{stat}}$ and G_{stat} are evaluated. As the singular part of the Green's functions is present in these auxiliary functions, the number of integration points needed for (5) will be higher than in (6).

Finally, the form of the total moment matrix would be the sum of the static moment matrix (5) and of the dynamic moment matrix (6) at each frequency point, written as follows:

$$Z_{mn} = Z_{mn}^{\text{stat}} + Z_{mn}^{\text{dyn}}. \tag{7}$$

In Section III-A, the computational cost of the different evaluation methods for an efficient filling of the moment matrix is studied.

C. Switching Between Different Green's Function Evaluation Methods

Throughout this work, it has been discussed that the filling of the moment matrix is the most computationally expensive step in the numerical modeling of practical devices. This high-computational cost is mainly due to the large number of Green's function evaluations that have to be performed. For this reason, it is necessary to choose the most efficient way to evaluate the Green's function in each case.

In order to make the proposed EFIE solution more efficient, it will be studied how to switch between the Ewald method and the modal summation method in the spectral domain, since it is very fast and accurate for relatively large electrical distances. The aim is to estimate a distance, in terms of the wavelength of the rectangular waveguide for the TE_{10} mode (λ_g), from which it is appropriate to use the series of Green's functions in the spectral domain. To determine when it is appropriate to switch between the two ways of evaluating the Green's functions, the time to evaluate them Green's functions is measured as the distance along the direction of propagation increases ($|z-z'|$), as shown in Fig. 6(a).

The specific details of the analysis are represented in the drawing of Fig. 6(a), where the working frequency is 10 GHz, the position of the source in the XY plane is $x' = 11.43$ mm and $y' = 5.08$ mm, and the observation point is located at $x = 11.43$ mm and $y = 5.082$ mm. The different Green's functions have been calculated for varying distance $|z - z'|$, at 200 points between 0 and $1.3\lambda_g$. The number of modes in both the Ewald method and the modal summation in the spectral domain varies dynamically with the distance along the direction of propagation to ensure a relative error in the Green's functions of less than 10^{-4}. In fact, this will cause the analysis time to change with distance, since as seen in [23] and [24], the number of modes needed in each case varies with the distance $|z - z'|$.

In Fig. 6(b), it can be seen that the analysis time of evaluating G_A^{zz} by means of modal summation in the spectral domain is very high for very small electrical distances. At these distances, it is necessary to take into account a high number of modes in the summation in order to ensure the desired relative error. Another aspect to note, and the reason why the abscissa axis starts at $|z - z'|/\lambda_g = 0.1$, is that this method does not converge to an optimal solution when the electrical distance is very close to 0, as explained in [23] and [24]. On the other hand, when the electrical distance is very large, it is sufficient to take into account only the propagative modes for the result to be accurate. It is for this reason that the analysis time converges to very small values when this electrical distance increases significantly. In the case of using the Ewald method to evaluate the Green's functions, the analysis time does not show such a strong dependence on the distance as the modal summation. However, in this method, there are complementary error functions that cause some inaccuracies in the results of the Green's functions when the electrical distances along the direction of propagation are very large. Therefore, as shown in Fig. 6(b), for distances larger than $|z-z'|/\lambda_g = 0.33$, it is more efficient and accurate to use the modal summation in the spectral domain to evaluate the Green's functions.

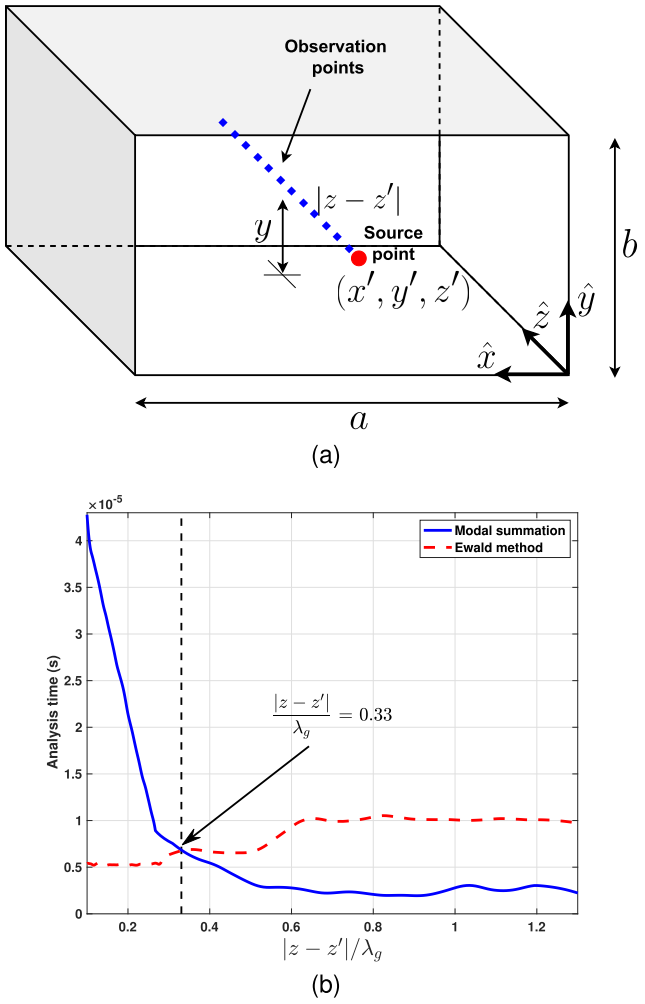

Fig. 6. (a) Sketch of a standard WR-90 rectangular waveguide, with cross-sectional dimensions $a = 22.86$ mm $\times$ $b = 10.16$ mm. This includes the location of a source point at coordinates $(x', y') = (11.43$ mm, 5.08 mm) and a distribution of observation points along the z-axis, at a height $y = 5.082$ mm from the bottom wall of the rectangular waveguide. (b) Analysis time of the G_A^{zz} component of the dyadic magnetic vector potential Green's function of the rectangular waveguide, when the distance along the propagation axis increases.

III. Results

This section will show some practical results of the theoretical concepts outlined in Section II. In Section III-A, the advantage of separating the moment matrix into static and dynamic parts will be studied. On the other hand, Section III-B will validate the complete formulation by calculating the scattering parameters of different conducting structures within a rectangular waveguide. Finally, in Section III-C, the different components of the electric and magnetic fields will be evaluated, and the results will be compared with those provided by the commercial ANSYS HFSS software.

A. Computational Cost of Different Options for Filling the Moment Matrix

In Section III-A, a study will be carried out with two different strategies to evaluate the elements of the static and

dynamic moment matrices. The challenge is to make the filling of the total impedance moment matrix as efficient as possible, but without compromising the accuracy of the results.

These two different strategies for evaluating the total impedance moment matrix are given as follows.

1) *Option 1:* No distinction is made between static and dynamic moment matrices. The elements of the matrix in which the Green's function becomes singular are solved by a transformation from rectangular to polar coordinates, able to cancel out the singular $(1/R)$ behavior of Green's functions. The computation of the Green's functions is accelerated by the Ewald method.
2) *Option 2:* A distinction is made between static (5) and dynamic (6) moment matrices. A discrete auxiliary static image distribution is used in the definition of the elements of the static moment matrix (see Fig. 2). The auxiliary distribution is composed up to the first layer of images, as shown in Fig. 2 (red, green, and blue dots). However, the source contribution $(1/R)$ is integrated analytically, and the remaining terms up to the first image layer are integrated numerically. On the other hand, in the dynamic moment matrix, the elements for which the dynamic Green's function is nondifferentiable are evaluated with the technique described in Fig. 5.

Note that in Option 2, the technique of dividing into subtriangles could be avoided by extracting one more term of the Taylor polynomial from the Green's function of the rectangular waveguide and integrating it also analytically, as in [32]. Even so, these cases only occur in the interaction between test and basis functions overlapping in the same mesh cell, as well as making the implementation a bit more complex.

The next step is to assess which of the above options is the most efficient one. For this, an example will be taken, in which we will have a rectangular waveguide with a metallic object inside. The objective will be to evaluate all the elements of the moment matrix for a frequency point. Note that in the case where a difference is made between static and dynamic moment matrix, the time of each matrix will be evaluated separately. Specifically, for this test, a standard WR-90 rectangular waveguide (with dimensions $a = 22.86$ mm $\times$ $b = 10.16$ mm), including a metallic cylinder centered with respect to the side walls, as shown in Fig. 7, is proposed. The working frequency for these examples is $f = 8$ GHz, and the number of basis and test functions of the structure shown in Fig. 7 is 366. The computer used has a 12-core Apple Silicon M2 Pro processor and 32 GB of RAM Memory.

Table I shows a comparison of the computational times using the two different options described previously for the evaluation of the static and dynamic moment matrices.

Results indicate that the most efficient method is the one corresponding to Option 2. Therefore, this will be the option to be used in the examples in Section III-B.

To conclude this section, it is also important to choose an optimal value for the number of integration points of the generalized impedance moment matrices. After a convergence study, it has been found that a maximum of nine integration points is sufficient to obtain accurate results.

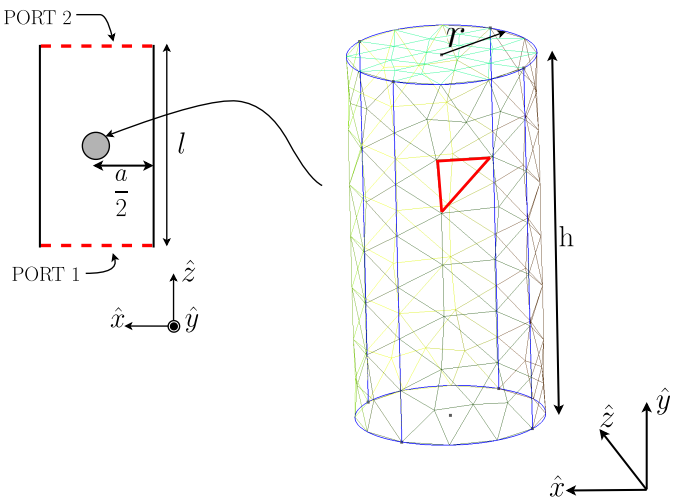

Fig. 7. Mesh of a circular cylinder provided by the GMSH software [33], whose radius is $r = 1.5$ mm and height $h = 6$ mm. The number of mesh cells is 236, and the number of basis and test functions is 366.

TABLE I

COMPUTATIONAL COST OF THE EVALUATION METHODS DESCRIBED IN SECTION III-A. IN THESE ANALYSES, A STANDARD WR-90 RECTANGULAR WAVEGUIDE OF DIMENSIONS $a = 22.86$ mm $\times$ $b = 10.16$ mm, WITH A CONDUCTING CIRCULAR POST INSIDE AND AN OPERATING FREQUENCY OF $f = 8$ GHz, HAS BEEN USED AS AN EXAMPLE. FOR THE ACCELERATED GREEN'S FUNCTIONS USING THE EWALD METHOD, TEN MODES AND AN IMAGE LAYER HAVE BEEN USED. THE SIZE OF THE MATRICES IS $N_c \times N_c$ ($N_c = 366$, NUMBER OF BASIS AND TEST FUNCTIONS). THE CHOSEN RELATIVE ERROR THRESHOLD IS LESS THAN 0.01

Calculation method	Computational cost (s)
Option 1	$Z_{mn}^{total} \rightarrow 1.62$
Option 2	$Z_{mn}^{stat} \rightarrow 0.291$ $\quad Z_{mn}^{dyn} \rightarrow 0.239$

B. Evaluation of the Scattering Parameters for Arbitrarily Shaped Conducting Structures in Rectangular Waveguide

In this section, all the theory outlined in Section II is applied, from filling the moment matrix efficiently (see Sections II-A–II-C), to the evaluation of the S-parameters (see Section II-D). Furthermore, Option 4 described in Section III-A will be used, as it was proved to be the most computationally efficient of all explored options.

The examples to be shown below consist of a rectangular waveguide perturbed by a number of arbitrarily shaped metallic elements. Furthermore, the examples will be validated with the help of the commercial ANSYS HFSS [28] and CST Studio Suite [29] full-wave software packages. For these analyses, the computer used is based on an Intel Core i7-6700K processor @4.00 GHz and 40 GB of RAM.

It should also be noted that for optimal performance, both in terms of accuracy and analysis time in our IE software, an appropriate mesh density must be chosen. In these examples, the mesh will have a maximum edge length of 0.1λ (where lambda is the wavelength of the medium filling the waveguide). Although, in some cases, a larger maximum edge length can be used, not in all configurations, this is enough

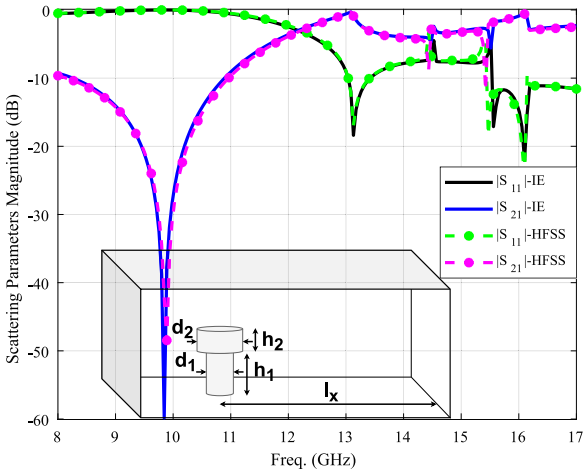

Fig. 8. Scattering parameters of a standard WR-90 rectangular waveguide of dimensions ($a = 22.86$ mm $\times$ $b = 10.16$ mm) with a metallic mushroom shaped inset. The mushroom is located at a distance $l_x = 9$ mm from the right wall and is centered with respect to the ports, the diameters are $d_1 = 2.6$ mm and $d_2 = 4.8$ mm, and the heights are $h_1 = 3.5$ mm and $h_2 = 2.5$ mm. The results provided by the proposed IE technique have been compared with those retrieved from the full-wave software ANSYS HFSS.

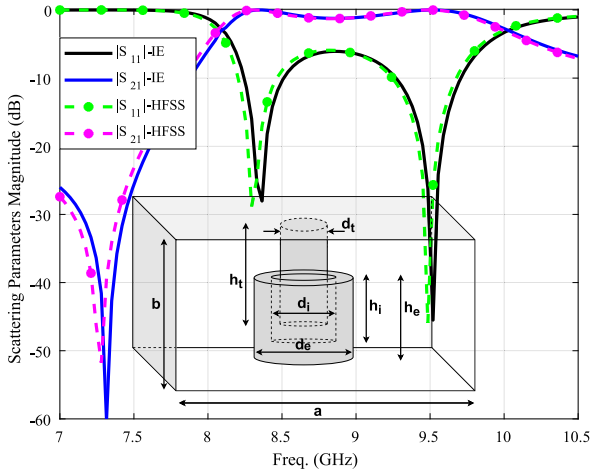

Fig. 9. Scattering parameters of a rectangular waveguide of dimensions ($a = 30$ mm $\times$ $b = 15$ mm) with a metallic reentrant post in a holed cylinder. Both the reentrant post and the cylinder are centered with respect to the input and output ports and the waveguide walls. The dimensions of the metallic cylinder are as follows: $h_e = 10$ mm, $h_i = 7$ mm, $d_i = 8$ mm, and $d_e = 12$ mm. The dimensions of the metallic re-entrant post are as follows: $h_t = 10$ mm and $d_t = 4$ mm. The results provided by the proposed IE technique have been compared with those obtained by the full-wave software ANSYS HFSS.

to achieve sufficiently accurate results, especially for rounded structures. Another alternative would be the use of basis functions defined on curvilinear elements [34], which would allow the mesh density to be reduced for rounded geometries. However, in this work, only test and basis functions of type RWG have been used for triangular mesh cells, and rooftop for rectangular mesh cells.

The first of the examples is a standard WR-90 rectangular waveguide with a mushroom-shaped metallic inset placed inside, as depicted in Fig. 8. In this example, to validate the expressions developed in Section II-D, the structure will be analyzed both in the monomode and in the multimode regions.

In this example, the number of basis functions needed in our IE software was 246, whereas in the worst case, the number of terms needed to achieve a reasonable convergence computing the Green's functions accelerated by the Ewald method was ten modes for the spectral part and one layer of images for the spatial contribution [23], [24]. This analysis has been carried out at 201 frequency points, resulting in an analysis time for the IE technique of 36 s. On the other hand, ANSYS HFSS took 20 min and 19 s. In Fig. 8, it is possible to observe a very good agreement between the results obtained by the proposed IE technique and those provided by the commercial software ANSYS HFSS.

The next validation example is a holed cylinder with a reentrant post, both metallic, inside a rectangular waveguide. The proposed topology (with geometrical dimensions) and the simulated scattering parameters can be seen in Fig. 9.

In this example, the number of basis functions needed in our IE software was 649, whereas the number of terms needed to accurately compute the Green's functions accelerated by the Ewald method was ten modes for the spectral part and only one image layer for the spatial contribution. This analysis has been carried out at 101 discrete frequency points, resulting in a computation time for the IE technique of 2 min and 24 s. In contrast, ANSYS HFSS took 16 min and 42 s for the same evaluation. As in the first example, the IE method proposed in this work yields a very good agreement when compared with ANSYS HFSS.

Finally, in Fig. 10, a first-order bandpass filter built in an evanescent mode rectangular waveguide can be observed. In this particular case, the filter is of the first order, being the resonator a metallic screw inserted in an evanescent field region, that allows mechanically tuning the resonant frequency. The purpose of this example is to show how this kind of structure should be meshed for optimum performance. The idea is to define, as the metallic obstacle, the evanescent waveguide region, including the tuning screw, inside a base waveguide of dimensions ($a \times b$). As expected, it would also be possible to analyze higher order filters, which would be meshed in a similar way as the bandpass filter sketched in Fig. 10. In this example, the filter will be analyzed for two different screw depths, with all other geometrical parameters remaining constant. This will allow the resonant cavity to be tuned at two different frequencies. In the caption of Fig. 10, we show all the dimensions of the structure, including the two screw depths.

In this case, the results have been compared with the commercial software CST, to further validate the results provided by our IE technique. In these analyses, the number of basis functions in the IE technique was 566 and 530 for the cases $h = 5.82$ mm and $h = 5.1$ mm, respectively. These analyses have been carried out at 101 frequency points. For the case with $h = 5.82$ mm, the analysis time took 1 min and 32 s for the IE technique and 12 min for CST. On the other hand, for $h = 5.1$ mm, the analysis time took 1 min and 22 s for the IE technique and 8 min and 27 s for CST. In Fig. 11, the results of these two analysis are shown. As can be seen, these results present a very good agreement between those obtained by the proposed IE technique and the commercial CST software.

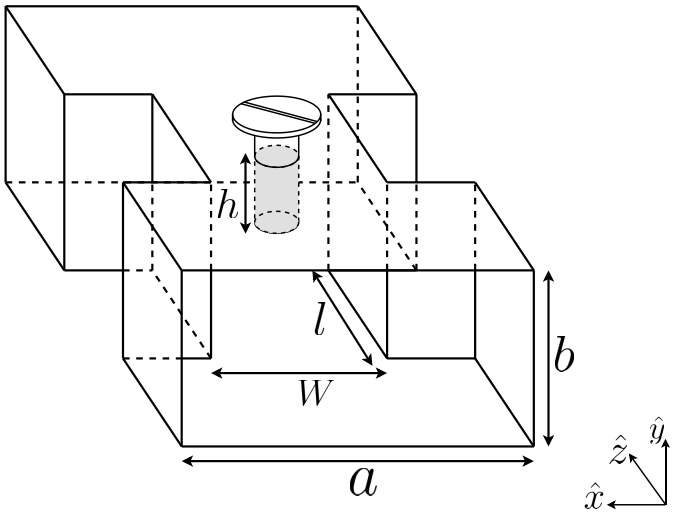

Fig. 10. Sketch of a standard WR-90 rectangular waveguide of dimensions (a = 22.86 mm × b = 10.16 mm), including an evenecesnt section whose width is W = 9 mm, and a resonator screw centered with respect to these walls. The length of the evanescent section is l = 8 mm, whereas the depth of the resonator screw will be h = 5.82 mm for a resonant frequency of f_0 = 9.5 GHz and h = 5.1 mm for a resonant frequency of f_0 = 10.5 GHz.

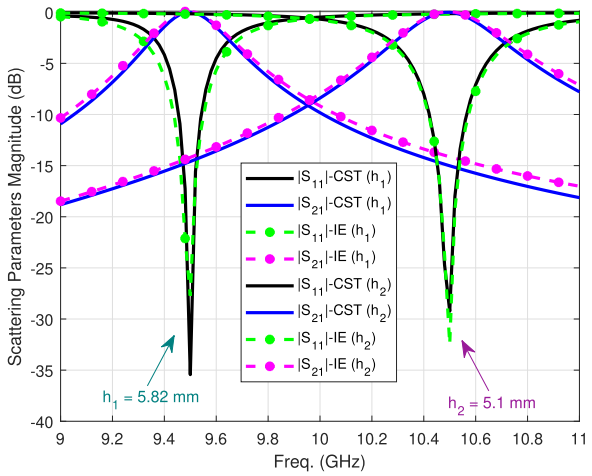

Fig. 11. Scattering parameters of an evanescent first-order bandpass filter built in a standard WR-90 rectangular waveguide of dimensions (a = 22.86 mm × b = 10.16 mm), as shown in Fig. 10. Results are shown for two different depths of the tuning screw. The metallic obstacle to be meshed is defined as the evanescent section of dimensions ($W \times b \times l$) together with the tuning screw.

C. Evaluation of Electromagnetic Fields Inside Rectangular Waveguides With Conducting Elements

As mentioned in this article, the derived formulation allows the electromagnetic fields to be evaluated in a relatively simple way inside the structures under analysis. This type of evaluation is very important in order to carry out studies on high-power phenomena, such as RF breakdown due to corona and multipactor [2], [3]. The expressions for the total electric and magnetic fields inside our structure are

$$\vec{E}^{\text{total}} = \vec{E}^{i} + \vec{E}^{s} \tag{8}$$

$$\vec{H}^{\text{total}} = \vec{H}^{i} + \vec{H}^{s} \tag{9}$$

where $\vec{E}^{i}$ and $\vec{H}^{i}$ are the incident electric and magnetic fields. On the other hand, $\vec{E}^{s}$ and $\vec{H}^{s}$ are the scattered electric and magnetic fields. In (1), the scattered electric field is written in the form of auxiliary potential functions, while the scattered magnetic field has the following form:

$$\vec{H}^{s} = \frac{1}{\mu}\left[\nabla \times \vec{A}\left(\vec{J}_c(\vec{r}\,')\right)\right]. \tag{10}$$

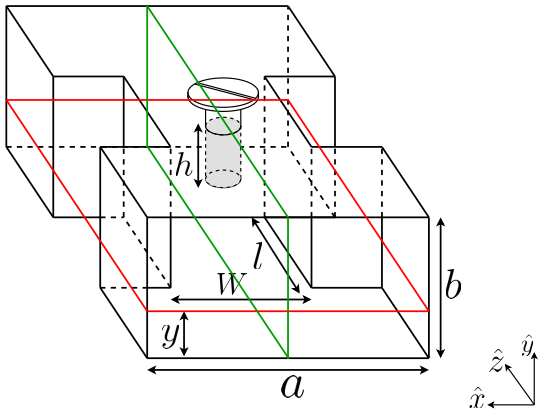

Fig. 12. Resonant cavity first depicted in Fig. 10, with the cut planes where the different components of the electric and magnetic fields will be evaluated. The XZ plane (with red borders) is located at a height y = 3 mm from the bottom wall of the filter. The electric field will be evaluated in this plane. The ZY plane (bordered in green) is located at $x = a/2$. In this plane, the magnetic field will be evaluated.

In this work, in order to validate the calculation of the electromagnetic fields inside guided structures, all the components of the electric and magnetic fields, produced by the TE_{10} mode excitation, will be evaluated inside the resonant cavity shown in Fig. 10. A schematic of the cut planes where the electric and magnetic fields will be evaluated can be seen in Fig. 12.

For the calculations, the same filter configuration, as shown in Fig. 12, will be used, where the screw depth will have a length of h_1 = 5.82 mm. The working frequency is 9.5 GHz, the number of basis functions used in this analysis is 566, the number of modes in the spectral contribution when using the Ewald method to evaluate the Green's functions is 10, and, in the spatial contribution, only one image layer has been taken into account [23], [24]. The number of points in each plane, where the different components of the electric and magnetic fields are evaluated, is 2500. The results are compared with those provided by ANSYS HFSS. On the other hand, it should be noted that a normalization process has been made in the formulation of the proposed IE technique, to assess the accuracy of the different components of the electric and magnetic fields. This is because ANSYS HFSS waveport excitation has a default power of 1 W. For this purpose, average power is calculated at the input port, for the TE_{10} mode and a given frequency, making use of the Poynting vector. After this evaluation, it is equated to the default power in ANSYS HFSS, and a relation between both methods is obtained to allow a correct comparison of the results.

This first calculation shows the magnitude of the y component of the electric field $|E_y|$ for the XZ oriented plane shown in Fig. 12. In Fig. 13, the objects that are traversing the plane in which the electric field is evaluated are shown in red solid line, while the object that is not being traversed by the plane is shown in dashed line. In this case, the plane where the electric

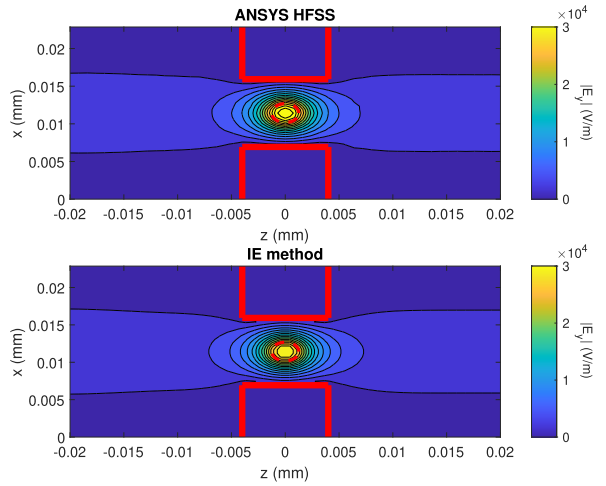

Fig. 13. $|E_y|$ component in an XZ plane within the structure shown in Fig. 12. The top image shows the results provided by ANSYS HFSS, while the bottom image shows the results obtained by the proposed IE method.

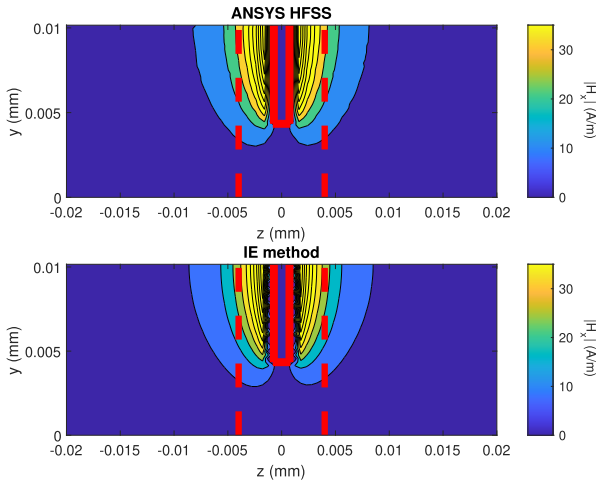

Fig. 14. $|H_x|$ component in an YZ plane within the filter in Fig. 12. The top image shows the results provided by ANSYS HFSS, while the bottom image shows the results obtained by the proposed IE method.

field is evaluated is below the metal screw. On the other hand, at the level of comparison of results, it can be seen that the IE technique proposed to evaluate the electric field presents a good agreement with the results provided by ANSYS HFSS.

As depicted in Fig. 14, in the second example, you can see the evaluation of the magnitude of the x component of the magnetic field $|H_x|$ in the plane with YZ orientation shown in Fig. 12. In this case, the plane where the different components of the magnetic field are evaluated passes through the metal screw, but not through the walls of the evanescent rectangular waveguide section. As in the previous example, the results obtained with the IE technique and the results provided by ANSYS HFSS are in good agreement.

To conclude this section, it can be seen that this is a simple option to obtain the different components of the electric and magnetic fields from the incident electric or magnetic field (which will have a known analytical form for the desired excitation mode) and the scattered electric or magnetic field. The latter ones are to evaluate once the unknowns of the EFIE technique proposed in this work have been solved.

IV. Conclusion

In this work, an EFIE formulation for the analysis of rectangular waveguide problems, including 3-D arbitrarily shaped conducting elements, has been implemented. Moreover, the filling of the moment matrix for solving the EFIE by the MoM has been optimized by separating the dynamic and static counterparts, improving the computational cost by a factor of 3 with respect to evaluating the moment matrix directly. The dynamic part, after subtracting the static part of the Green's functions and thus obtaining a smooth behavior, has been evaluated with a reduced number of integration quadrature points, in addition to evaluating the Green's functions by applying the Ewald method to speed up the calculations. On the other hand, in the static moment matrix, the optimal solution found in this work to efficiently evaluate the self interaction between base and test functions defined on the same mesh cell is based on the analytical integration of the source contribution $(1/R)$ that models the singular behavior of the Green's functions. Another aspect to highlight is the study carried out to evaluate the Green's functions, present in the moment matrix, in the most efficient possible way as a function of the electrical distance. Also, a generic expression has been outlined for the evaluation of the multimode scattering parameters, so that it is possible to measure the coupling of different modes at the input/output ports of the rectangular waveguide circuits. Finally, with these advances, it is possible to carry out the analysis of 3-D complex microwave circuits in guided technology, with a reduced computational cost compared with other alternatives, such as ANSYS HFSS, which has been the software used to estimate the accuracy of the proposed technique. In addition, electromagnetic fields inside guided structures can also be evaluated in a simple way. As a future line of research, the extension of this IE formulation to the analysis of step discontinuities between rectangular waveguides, to the presence of dielectric objects inside rectangular waveguides, or even to the concatenation of different structures in guided technology, such as the concatenation of rectangular waveguides with rectangular cavities, can be considered.

References

[1] R. J. Cameron, C. M. Kudsia, and R. R. Mansour, *Microwave Filters for Communication Systems: Fundamentals, Design and Applications*, 2nd ed. Hoboken, NJ, USA: Wiley, Mar. 2018.

[2] A. R. Perez, A. P. Abenza, F. D. Q. Pereira, J. H. Jimenez, A. A. Melcon, and J. S. G. Diaz, "A novel low-pass filter based on dielectric impedance inverters to enhance the multipactor breakdown threshold," *AEU Int. J. Electron. Commun.*, vol. 143, Jan. 2022, Art. no. 154040.

[3] T. Pinheiro-Ortega et al., "Microwave corona breakdown prediction in arbitrarily-shaped waveguide based filters," *IEEE Microw. Wireless Compon. Lett.*, vol. 20, no. 4, pp. 214–216, Apr. 2010, doi: 10.1109/LMWC.2010.2042555.

[4] M. Taroncher et al., "CAD of complex passive devices composed of arbitrarily shaped waveguides using Nyström and BI-RME methods," *IEEE Trans. Microw. Theory Techn.*, vol. 53, no. 6, pp. 2153–2163, Jun. 2005, doi: 10.1109/TMTT.2005.848795.

[5] R. R. Mansour, "Filter technologies for wireless base stations," *IEEE Microw. Mag.*, vol. 5, no. 1, pp. 68–74, Mar. 2004, doi: 10.1109/MMW.2004.1284945.

[6] V. Boria and B. Gimeno, "Waveguide filters for satellites," *IEEE Microw. Mag.*, vol. 8, no. 5, pp. 60–70, Oct. 2007.

[7] S. D. Gedney, *Introduction to the Finite-Difference Time-Domain (FDTD) Method for Electromagnetics* (Synthesis Lectures on Computational Electromagnetics). Switzerland: Springer, 2011.

[8] M. Salazar-Palma, T. K. Sarkar, L.-E. Garcia-Costillo, T. Roy, and A. Djordjevic, *Iterative and Self-Adaptive Finite Elements in Electromagnetic Modeling*. Norwood, MA, USA: Artech House, 1998.

[9] A. F. Peterson, S. L. Ray, and R. Mittra, *Computational Methods for Electromagnetics*, vol. 24. New York, NY, USA: IEEE Press, 1998.

[10] R. F. Harrington and J. L. Harrington, *Field Computation by Moment Methods*. London, U.K.: Oxford Univ. Press, 1996.

[11] M. Guglielmi and C. Newport, "Rigorous, multimode equivalent network representation of inductive discontinuities," *IEEE Trans. Microw. Theory Techn.*, vol. 38, no. 11, pp. 1651–1659, Nov. 1990.

[12] C. G. Molina, F. Q. Pereira, A. A. Melcón, V. E. Boria, and M. Guglielmi, "An efficient technique to assess the convergence of the multimode equivalent network for waveguide devices," *IEEE Trans. Microw. Theory Techn.*, vol. 66, no. 2, pp. 651–659, Feb. 2018.

[13] C. G. Molina et al., "Multimode equivalent network for boxed multilayer arbitrary planar circuits," *IEEE Trans. Microw. Theory Techn.*, vol. 68, no. 7, pp. 2501–2514, Jul. 2020.

[14] C. T. Vincenzo, M. Mongiardo, and C. Tomassoni, "Efficient CAD of a class of waveguide discontinuities via an hybrid finite-element/mode-matching and modified transverse-resonance analysis," in *IEEE MTT-S Int. Microw. Symp. Dig.*, Jun. 2003, pp. 1223–1226.

[15] J. M. Reiter and F. Arndt, "Rigorous analysis of arbitrarily shaped H- and E-plane discontinuities in rectangular waveguides by a full-wave boundary contour mode-matching method," *IEEE Trans. Microw. Theory Techn.*, vol. 43, no. 4, pp. 796–801, Apr. 1995.

[16] F. Mira, M. Bressan, G. Conciauro, B. G. Martinez, and V. E. B. Esbert, "Fast S-domain modeling of rectangular waveguides with radially symmetric metal insets," *IEEE Trans. Microw. Theory Techn.*, vol. 53, no. 4, pp. 1294–1303, Apr. 2005.

[17] P. Arcioni, M. Bozzi, M. Bressan, G. Conciauro, and L. Perregrini, "Frequency/time-domain modelling of 3D waveguide structures by a BI-RME approach," *Int. J. Numer. Model. Electron. Netw., Devices Fields*, vol. 15, no. 1, pp. 3–21, Jan. 2002.

[18] P. Arcioni, M. Bozzi, M. Bressan, and L. Perregrini, "A novel CAD tool for the wideband modeling of 3D waveguide components," *Int. J. RF Microw. Comput.-Aided Eng.*, vol. 10, no. 3, pp. 183–189, May 2000. [Online]. Available: https://onlinelibrary.wiley.com/doi/abs/10.1002/%28SICI%291099-047X%28200005%2910%3A3%3C183%3A%3AAID-MMCE5%3E3.0.CO%3B2-C

[19] S. Rao, *Electromagnetic Scattering and Radiation of Arbitrarily-Shaped Surfaces by Triangular Patch Modeling*. Ann Arbor, MI, USA: University Microfilms, 1984.

[20] A. Glisson and D. Wilton, "Simple and efficient numerical methods for problems of electromagnetic radiation and scattering from surfaces," *IEEE Trans. Antennas Propag.*, vol. AP-28, no. 5, pp. 593–603, Sep. 1980.

[21] S. Rao, D. Wilton, and A. Glisson, "Electromagnetic scattering by surfaces of arbitrary shape," *IEEE Trans. Antennas Propag.*, vol. AP-30, no. 3, pp. 409–418, May 1982.

[22] R. E. Collin, *Field Theory of Guided Waves, Chapter 5-Waveguides and Cavities*. Hoboken, NJ, USA: Wiley, 1990, pp. 329–410.

[23] M.-J. Park and S. Nam, "Rapid summation of the Green's function for the rectangular waveguide," *IEEE Trans. Microw. Theory Techn.*, vol. 46, no. 12, pp. 2164–2166, Dec. 1998.

[24] A. M. H. de la Cruz, C. G. Molina, F. D. Q. Pereira, A. Á. Melcón, and V. E. B. Esbert, "Efficient calculation of the 3-D rectangular waveguide Green's functions derivatives by the Ewald method," *IEEE Trans. Microw. Theory Techn.*, vol. 71, no. 12, pp. 5171–5181, Dec. 2023.

[25] P. Arcioni, M. Bressan, and L. Perregrini, "On the evaluation of the double surface integrals arising in the application of the boundary integral method to 3-D problems," *IEEE Trans. Microw. Theory Techn.*, vol. 45, no. 3, pp. 436–439, Mar. 1997.

[26] F. J. P. Soler, F. D. Q. Pereira, A. A. Melcon, B. Gimeno, V. E. B. Esbert, and L. Perregrini, "Analytical evaluation of the static MoM terms for volume and surface rectangular domains," *IEEE Antennas Wireless Propag. Lett.*, vol. 9, pp. 87–90, 2010.

[27] R. Cools, "Monomial cubature rules since 'stroud': A compilation—Part 2," *J. Comput. Appl. Math.*, vol. 112, nos. 1–2, pp. 21–27, Nov. 1999, doi: 10.1016/s0377-0427(99)00229-0.

[28] *ANSYS HFSS Software*. Accessed: Apr. 2024. [Online]. Available: https://www.ansys.com/products/electronics/ansys-hfss

[29] *CST Software*. Accessed: Apr. 2024. [Online]. Available: https://www.3ds.com/products/simulia/cst-studio-suite

[30] P. M. Harman and J. C. Maxwell, "The scientific letters and papers of James Clerk Maxwell, volume II: 1862–1873," *Brit. J. Philosophy Sci.*, vol. 47, no. 4, pp. 654–657, 1996.

[31] J. R. Mosig, "Arbitrarily shaped microstrip structures and their analysis with a mixed potential integral equation," *IEEE Trans. Microw. Theory Techn.*, vol. MTT-36, no. 2, pp. 314–323, Feb. 1988.

[32] P. Yla-Oijala and M. Taskinen, "Calculation of CFIE impedance matrix elements with RWG and n× RWG functions," *IEEE Trans. Antennas Propag.*, vol. 51, no. 8, pp. 1837–1846, Aug. 2003.

[33] C. Geuzaine and J.-F. Remacle, "Gmsh: A 3-D finite element mesh generator with built-in pre- and post-processing facilities," *Int. J. Numer. Methods Eng.*, vol. 79, no. 11, pp. 1309–1331, Sep. 2009.

[34] L. Valle, F. Rivas, and M. F. Catedra, "Combining the moment method with geometrical modelling by NURBS surfaces and Bezier patches," *IEEE Trans. Antennas Propag.*, vol. 42, no. 3, pp. 373–381, Mar. 1994.

Antonio Manuel Huéscar de la Cruz (Student Member, IEEE) was born in Murcia, Spain, in 1997. He received the bachelor's degree in telecommunication systems and the master's degree in telecommunication engineering from the Technical University of Cartagena (UPCT), Cartagena, Spain, in 2019 and 2021, respectively.

In 2021, he joined the Department of Information and Communication Technologies, UPCT, as a Researcher, where he currently develops his Ph.D. research activity. He is involved in the development of analytical and numerical tools for the analysis of microwave circuits in waveguide technology.

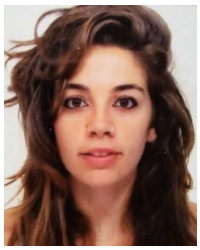

Celia Gómez Molina was born in Murcia, Spain, in 1992. She received the bachelor's degree in telecommunication systems and the master's degree in telecommunication engineering from the Technical University of Cartagena (UPCT), Cartagena, Spain, in 2014 and 2016, respectively, and the Ph.D. degree from UPC, Barcelona, Spain, in 2020.

In 2016, she joined the Department of Information Technologies and Communications, UPCT, as a Researcher, where she developed her teaching and Ph.D. research activities. She was a Visiting Student with the University of California at Davis, Davis, CA, USA, in 2018, and the Politecnico di Milano, Milan, Italy, in 2019. She is involved in the development of analytical and numerical tools for network representations of waveguide and planar discontinuities. Her current scientific interests include the design of microwave filters using different technologies.

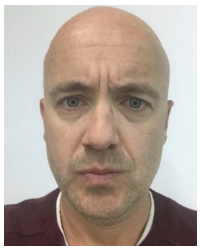

Fernando Daniel Quesada Pereira (Member, IEEE) was born in Murcia, Spain, in 1974. He received the master's degree in telecommunications engineering from the Technical University of Valencia (UPV), Valencia, Spain, in 2000, and the Ph.D. degree from the Technical University of Cartagena (UPCT), Cartagena, Spain, in 2007.

In 1999, he joined the Department of Radiocommunications, UPV, as a Research Assistant, where he was involved in the development of numerical methods for the analysis of anechoic chambers and tag antennas. In 2001, he joined the Department of Communications and Information Technologies, UPCT, as a Research Assistant, and then as an Assistant Professor. In 2005, he was a Visiting Scientist with the University of Pavia, Pavia, Italy. In 2009, he was an Invited Researcher with UPV. In 2011, he became an Associate Professor with UPCT. His current research interests include integral equation numerical methods for the analysis of antennas and microwave devices, along with microwave filters design and applications.

Alejandro Álvarez Melcón (Senior Member, IEEE) was born in Madrid, Spain, in 1965. He received the master's degree in telecommunications engineering from the Technical University of Madrid (UPM), Madrid, in 1991, and the Ph.D. degree in electrical engineering from ETH Zürich, Lausanne, Switzerland, in 1998.

In 1988, he joined the Department of Signal, Systems and Radiocommunications, UPM, as a Researcher, where he was involved in the design, testing, and measurement of broadband spiral antennas for electromagnetic measurements support equipment. From 1991 to 1993, he was with the Radio Frequency Systems Division, European Space Agency (ESA/ESTEC), Noordwijk, The Netherlands, where he was involved in the development of analytical and numerical tools for the study of waveguide discontinuities, planar transmission lines, and microwave filters. From 1993 to 1995, he was with the Space Division, Industry Alcatel Espacio, Madrid, and ESA, where he collaborated in several ESA/European Space Research and Technology Centre contracts. From 1995 to 1999, he was with ETH Zürich, École Polytechnique Fédérale de Lausanne, Lausanne, where he was involved in the field of microstrip antennas and printed circuits for space applications. In 2000, he joined the Technical University of Cartagena, Cartagena, Spain, where he is currently developing his teaching and research activities. He was an Invited Professor with Polytechnique Montréal, Montreal, QC, Canada, in 2010, and a Visiting Professor with the University of California at Davis, Davis, CA, USA, from 2017 to 2018.

Dr. Álvarez Melcón was a recipient of the Journée Internationales de Nice Sur les Antennes (JINA) Best Paper Award for the best contribution to the JINA'98 International Symposium on Antennas and the Colegio Oficial de Ingenieros de Telecomunicación Award to the best Ph.D. dissertation in basic information and communication technologies.

Vicente E. Boria Esbert (Fellow, IEEE) was born in Valencia, Spain, in 1970. He received the master's (Hons.) and Ph.D. degrees in telecommunications engineering from the Universidad Politécnica de Valencia, Valencia, in 1993 and 1997, respectively.

In 1993, he joined the Departamento de Comunicaciones, Universidad Politécnica de Valencia, where he has been a Full Professor since 2003. In 1995 and 1996, he was holding a Spanish trainee position with the European Space Research and Technology Centre, European Space Agency, Noordwijk, The Netherlands, where he was involved in the area of electromagnetic analysis and design of passive waveguide devices. He has authored or coauthored 15 chapters in technical textbooks, 200 articles in refereed international technical journals, and over 250 articles in international conference proceedings. His current research interests include the analysis and automated design of passive components, particularly in filters and multiplexers, several technologies, and the simulation and measurement of power effects in high-frequency devices and systems.

Dr. Boria Esbert has been a member of the IEEE Microwave Theory and Techniques Society (IEEE MTT) and the IEEE Antennas and Propagation Society since 1992. He is currently a member of the European Microwave Association (EuMA). He is also an Editorial Board Member of the *International Journal of RF and Microwave Computer-Aided Engineering* and a member of the Technical Committees of the IEEE-MTT International Microwave Symposium and the European Microwave Conference. He has been the Chair for the 48th European Microwave Conference held in Madrid. He acts as a regular reviewer of the most relevant IEEE and IET technical journals on his areas of interest. He was an Associate Editor of the IEEE MICROWAVE AND WIRELESS COMPONENTS LETTERS from 2013 to 2018 and the *IET Electronics Letters* from 2015 to 2018. He currently serves as a Subject Editor for the *IET Electronics Letters* (Microwaves).